THE ASTROPHYSICAL JOURNAL, 440:888–893, 1995 February 20

TESTING THE DC–ELECTRIC FIELD MODEL IN A SOLAR FLARE OBSERVED BY *YOHKOH* AND THE *COMPTON GAMMA-RAY OBSERVATORY*

D. M. ZARRO,[1] J. T. MARISKA,[2] AND B. R. DENNIS[3]

Received 1994 February 22; accepted 1994 September 2

ABSTRACT

We apply a DC–electric field model to the analysis of soft and hard X-ray observations of a solar flare observed by *Yohkoh* and the *Compton Gamma-Ray Observatory CGRO* on 1992 September 6. The flare was observed simultaneously in the soft X-ray Ca XIX line by the *Yokhoh* Bragg Crystal Spectrometer (BCS) and in hard X-rays (>50 keV) by the *CGRO* Burst and Transient Spectrometer Experiment (BATSE). A strong stationary component of Ca XIX emission was present at the start of impulsive hard X-ray emission indicating an extended phase of heating prior to the production of energetic nonthermal electrons. We interpret the preflare Ca XIX emission as a signature of Joule heating by field-aligned currents. We relate the temporal variation of impulsive hard X-ray emission to the rate of runaway electron acceleration by the DC–electric field associated with the current. We find that the initial rise in hard X-ray emission is consistent with electron acceleration by a DC–electric field that increased from a preflare value of $\lesssim 10^{-5}$ V cm^{-1} to $\simeq (9 \pm 1) \times 10^{-5}$ V cm^{-1} at the time of the first hard X-ray peak and then remained constant during the rest of the impulsive phase. We attribute the increase in electric field strength to the formation of a current sheet at the reconnection point of two loop structures. The decrease in hard X-ray emission after flare maximum is consistent with a reduction in the number of runaway electrons due to an increase in coronal density produced by chromospheric evaporation. The increased density quenches the runaway process by enhancing collisional thermalization of electrons. To avoid the generation of an unrealistically large magnetic field, the flaring region must be highly filamented into $\gtrsim 10^6$ oppositely directed current channels of ~ 30 cm width with an initial preflare current of $\simeq 3 \times 10^{10}$ A per channel.

Subject headings: MHD — Sun: flares — Sun: X-rays, gamma rays

1. INTRODUCTION

Electric currents and their associated electric fields have been shown to provide a viable mechanism for heating plasma and for accelerating particles in solar flares (Tsuneta 1985; Holman 1985; Moghaddam-Taaheri & Goertz 1990). In particular, quasi-static DC–electric fields parallel to the coronal magnetic field can accelerate thermal electrons until a steady state current is established. Since the collisional drag on the electrons decreases with increasing velocity, the electrons with velocities above a critical velocity will undergo runaway acceleration to superthermal energies (Dreicer 1959; Spicer 1982). These runaway electrons can produce significant nonthermal hard X-ray (HXR) emission via thick-target interactions (Holman 1985; Holman, Kundu, & Kane 1989). Electrons with velocities below the threshold for runaway acceleration continue to heat the ambient plasma (via Joule heating) thereby producing thermal soft X-ray emission. Hence, an attractive feature of electric fields is the potential for simultaneously explaining thermal and nonthermal processes occurring in solar flares.

The mechanism for producing coronal electric fields is a subject of considerable debate. It is widely believed that such fields are generated by magnetic instabilities and reconnection processes that are involved in the triggering of a solar flare (cf. Tandberg-Hanssen & Emslie 1988). Numerical studies suggest a scenario in which electric field structures may be produced in coronal magnetic field configurations that are sheared progressively by photospheric footpoint displacements (Roumeliotis, Sturrock, & Antiochos 1994). This physical connection between loop current systems and flare phenonema is reinforced observationally by high-quality vector magnetograph data that have revealed a close spatial association between vertical current components and Hα electron precipitation sites in the chromosphere (Canfield et al. 1993).

In this paper, we present new results obtained using a DC–electric field model to interpret simultaneous soft and hard X-ray observations of a flare obtained by instruments onboard the Japanese *Yohkoh* and *Compton Gamma-Ray Observatory* (*CGRO*) spacecraft. The increased spectral sensitivities of these instruments (relative to similar detectors on preceding spacecraft such as *SMM*) permit a study of the crucial early rise phase of the flare impulsive phase when signatures of plasma heating and particle acceleration are expected to be most revealing.

2. OBSERVATIONS

A *GOES*-class M3.3 flare occurred at 08:57 UT on 1992 September 6 in Active Region AR 7270 located at S11 W38. The flare was one of a series of events in this active region that was well-observed by *Yohkoh* (Shibata et al. 1993). It was observed simultaneously in the soft X-ray Ca XIX (3.17 Å) line by the *Yohkoh* Bragg Crystal Spectrometer (BCS) and in hard X-rays by the *CGRO* Burst and Transient Source Experiment (BATSE).

The BATSE instrument (Fishman et al. 1989) consists of eight detector modules. Each module contains two NaI scintillation detectors: a Large Area Detector (LAD) and a Spectroscopy Detector (SD). Figure 1*a* shows the evolution of the

[1] Applied Research Corp., Solar Data Analysis Center, Code 682 NASA/GSFC, Greenbelt, MD 20771.
[2] Naval Research Laboratory, Code 7673 Washington, DC 20375.
[3] Laboratory for Astronomy and Solar Physics, Code 682.2 NASA/GSFC, Greenbelt, MD 20771.

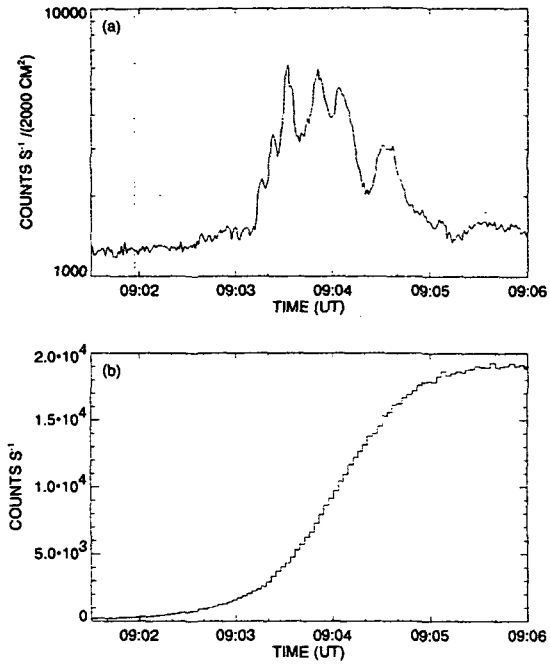

FIG. 1.—(*a*) The BATSE Discriminator Large Area (DISCLA) hard X-ray count rate for the 50–100 keV channel plotted at 1.024 s time resolution. The vertical dotted lines mark the accumulation interval of the BCS Ca XIX preflare spectrum plotted in Fig. 2.

Discriminator Large Area (DISCLA) hard X-ray count rate (1.024 s temporal resolution) in the 50–100 keV channel of the most sunward-facing LAD. Significant HXR emission was first detected at 09:02 UT. The emission reached a maximum at 09:03:31 UT and was followed by three successive bursts each 15–20 s in duration.

The BCS (Culhane et al. 1991) is an uncollimated full-Sun field-of-view spectrometer that consists of four detector channels that span narrow wavelength ranges centered on emission

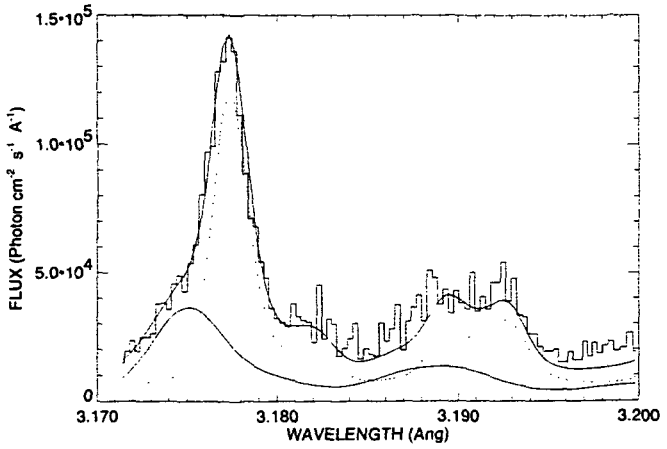

FIG. 2.—The BCS Ca XIX spectrum (15 s accumulation) at 09:01:57 UT, the approximate time when the first significant increase in BATSE hard X-ray emission above 50 keV was detected. The smooth solid line superposed on the spectrum is a two-component synthetic fit to the Ca XIX resonance and satellite lines. The dotted line indicates the stationary component. The underlying smooth line is the blueshifted component. The wavelength scale of the Ca XIX spectrum was calibrated by centering the resonance line during the late decay phase of the flare at the laboratory rest wavelength of 3.177 Å.

lines of highly ionized Fe XXVI, Fe XXV, Ca XIX, and S XV. The nominal temporal resolution of the spectra is 3 s. Figure 1*b* shows the light curve of the total count rate in the Ca XIX channel. Enhanced Ca XIX emission was observed 2–3 minutes before the peak of hard X-rays, with a strong stationary resonance line component (Fig. 2) already present at 09:01:57 UT–the approximate start time of hard X-rays.

2.1. *Flare Geometry*

We use 119 μm Be filter (centered on ≈ 10 Å) partial frame images from the *Yohkoh* Soft X-ray Telescope (SXT) to infer the geometry of the flare region. Figure 3 (Plate 11) shows a sequence of the available Be images during the interval 09:02:24–09:03:56 UT, corresponding to the rise phase of hard X-rays. To facilitate relative comparisons, the images have been renormalized to the peak intensity of the last image in the sequence. These images indicate that the soft X-ray emission originated in an approximately symmetric east-west (E-W) oriented looplike structure that was brightest initially at its center. At ~09:03:04 UT, the western leg of the loop brightened and eventually dominated the total emission from the loop structure. Hard X-ray images (>50 keV) obtained with the *Yohkoh* Hard X-ray Telescope (HXT) indicate that the impulsive phase burst emission occurred at the footpoints (denoted A and B) of the E-W loop structure (Yaji et al. 1993).

The spatial and temporal sequences of soft and hard X-ray brightenings suggest a geometry in which the smaller E-W soft X-ray loop interacted with a larger overlying loop structure (with footpoints denoted by C and B in Fig. 3). This situation is similar to the emerging flux model discussed by Heyvaerts, Priest, & Rust (1977). Accordingly, we identify the apex of the smaller loop as the energy release site at which electrons were initially accelerated and subsequently propagated to the footpoints to produce thick-target hard X-ray emission. The separation of the footpoints A and B is approximately $d \approx 28''.5$. Assuming a semicircular geometry, we deduce a corresponding half-length of $L_{obs} = \pi d/2 \simeq 3.2 \times 10^9$ cm for the E-W loop. We estimate the cross-sectional area of the E-W loop by computing the average width w along the region of soft X-ray emission connecting the A and B footpoints. Assuming a cylindrical loop volume and equating w with the loop diameter, we infer a cross-sectional area $A_{obs} = \pi w^2/4 \simeq 2.0 \times 10^{17}$ cm^2 and a total volume $V_{obs} = 2A_{obs} L_{obs} \simeq 1.3 \times 10^{27}$ cm^3.

2.2. *Flare Energetics*

We determine the electron temperature T_e of the stationary soft X-ray plasma from the relative intensities of the Ca XIX resonance and dielectronic satellite lines (Bely-Dubau et al. 1982). The line strengths are computed using a least-squares technique to fit synthetic profiles to the Ca XIX spectra (cf. Fludra et al. 1989). Figure 2 shows a fitted synthetic spectrum superposed on the observed preflare spectrum at 09:01:57 UT. The spectral fit implies a preflare temperature $T_e = (13 \pm 2) \times 10^6$ K and a corresponding preflare emission measure of $EM = \int n_e^2 dV = (5 \pm 2) \times 10^{47}$ cm^{-3}. Using the loop volume estimated from the SXT images and assuming a unity filling factor (see § 3), we derive the characteristic density $n_e \simeq [(EM/V_{obs})]^{1/2}$ of the loop. The evolutions of T_e and n_e during the impulsive phase are plotted in Figures 4*a* and 4*b*, respectively.

The Ca XIX spectra for this flare were exceptional because of a strong blue asymmetry that was evident before the peak of

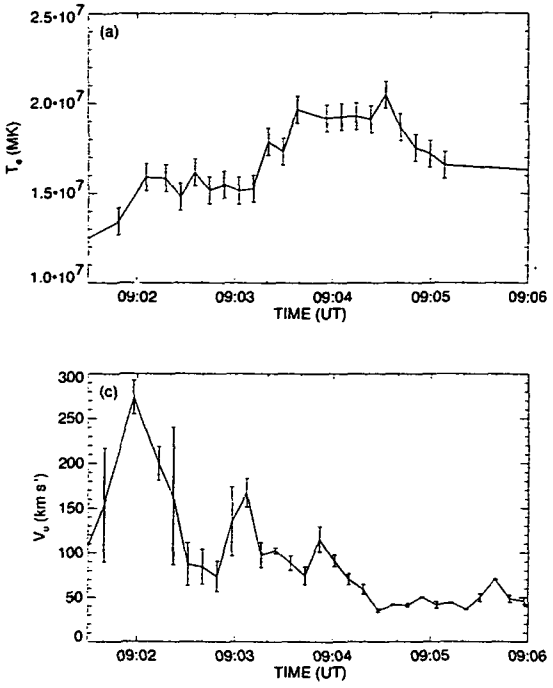

FIG. 4.—(*a*) The electron temperature of the soft X-ray plasma deduced from fits of synthetic spectra to the BCS Ca XIX resonance and satellite line profiles. To improve the signal-to-noise of each fit, the observed spectra were accumulated into 9 s intervals. (*b*) The electron density of the loop soft X-ray plasma deduced from the Ca XIX emission measure assuming a simple loop geometry and a unity filling factor. (*c*) The line-of-sight blueshift velocity deduced from the separation between the primary Ca XIX resonance line and the secondary component. Note the first velocity peak at 09:02 UT (before significant HXR emission) and the secondary peak at 09:03:10 UT (during the HXR rise phase).

hard X-rays. We have modeled the asymmetry by including a blueshifted component in the above least-squares fitting analysis. Figure 2 shows the resulting two-component fit to the preflare spectrum at 09:01:57 UT. The separation of the stationary and blueshifted components indicates an initial line-of-sight upflow velocity of $v \approx 270$ km s^{-1} at the time of the preflare spectrum. Figure 4*c* shows the evolution of the blueshift velocity during the impulsive phase. The upflow shows a secondary peak at 09:03:10 UT. To within the 9 s resolution of the BCS, this peak corresponds to the time when the SXT E-W loop feature showed enhanced brightening in the western leg. This temporal association suggests that the loop brightening was produced by gradual filling of the loop leg by chromospheric evaporation of soft X-ray plasma from the footpoint closest to the interaction site.

We compute the thermal heating rate $Q_{\rm obs}$ needed to sustain the soft X-ray emission from the loop by using the formula

$$Q_{\rm obs} = dU/dt + P_{\rm rad} + P_{\rm cond} \text{ ergs s}^{-1}, \quad (1)$$

where $U = 3n_e kT_e V_{\rm obs}$ is the total thermal energy of the plasma, $P_{\rm cond} \approx 10^{-6} T_e^{7/2} (2A_{\rm obs}/L_{\rm obs})$ is the classical conductive loss rate, and $P_{\rm rad} \approx 1.5 \times 10^{-19} n_e^2 T_e^{-1/2} V_{\rm obs}$ is the radiative loss rate (Antonucci, Gabriel, & Dennis 1984). The factor of 2 accounts for the assumed symmetry of the loop. Figure 5*a* shows the temporal variations of each of the terms in equation (1). Figure 5*b* shows the corresponding variation of $Q_{\rm obs}$. Note that the radiative loss term is negligible relative to the conductive term during the flare. For sufficiently strong heating, the resulting high-temperature gradients can produce free-streaming electrons that carry the conductive flux. In this case, the conductive flux is given by the saturated flux $F_{\rm sat} \approx \frac{1}{4} n_e m_e v_e^3$, where m_e is the electron mass and $v_e = (kT/m_e)^{1/2}$ is the electron thermal velocity (Manheimer & Klein 1975). The variation of $P_{\rm sat} = 2A_{\rm obs} F_{\rm sat}$ is shown in Figure 5*a*. Since the classical conductive term is below the saturated value for the adopted values of T_e and n_e, we use the classical term in equation (1). An additional limitation on the heat flux arises when bulk streaming of the electrons sets up ion-acoustic waves which enhance the collision frequency. In this case, the conductive flux is given by the anomalously limited heat flux (Tandberg-Hanssen & Emslie 1988). In § 3, we find that this anomalous-heating effect is not expected to be significant for the flare under study.

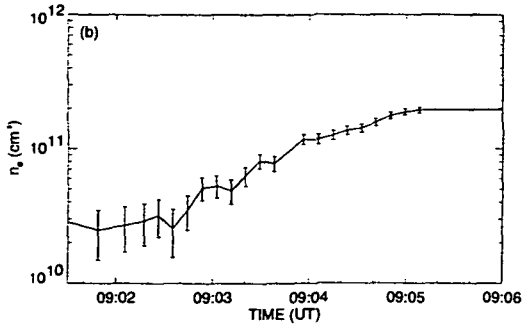

3. ANALYSIS

The 1992 September 6 flare is typical of many flares observed by *Yohkoh* in that it showed evidence of strong high-

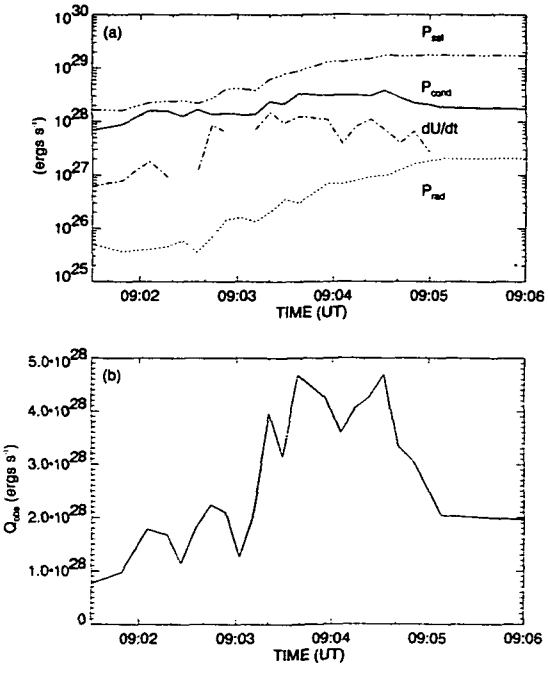

FIG. 5.—(*a*) The computed time rate of change of the thermal energy dU/dt in a loop with uniform temperature and density derived from BCS Ca XIX observations. The classical conductive $P_{\rm cond}$ and radiative $P_{\rm rad}$ energy-loss rates, as well as the saturated conductive loss rate $P_{\rm sat}$ are shown for comparison. (*b*) The total heating rate of the soft X-ray plasma $Q_{\rm obs} = dU/dt + P_{\rm cond} + P_{\rm rad}$. For the Ca XIX–derived temperatures and densities, the heating rate is dominated by the classical conductive loss term.

temperature Ca XIX emission before the onset of impulsive hard X-rays (Mariska et al. 1993). Again, as is typical in many flares, this stationary component was accompanied by a weaker blueshifted component which indicates evaporative upflows that commenced prior to the HXR impulsive phase. Similar behaviors were found in flares observed by *SMM* (Doschek et al. 1986; McClements & Alexander 1989). These observations place severe constraints on models of solar flares. For example, the thick-target driven chromospheric evaporation model predicts that the blueshifted component will initially *dominate* the Ca XIX profile when the plasma is being heated and evaporated by energetic electrons (Mariska, Emslie, & Li 1989; Li, Emslie, & Mariska 1990).

The presence of a dominant preflare stationary Ca XIX component appears to contradict the thick-target electron beam model unless some additional form of preflare heating is invoked (Mariska & Zarro 1991). If this heating is purely thermal in origin, then equation (1) implies a plasma heating rate of $Q_{obs} = 2 \times 10^{28}$ ergs s^{-1} before any significant hard X-ray emission was observed in the 1992 September 6 flare. The cause of this preflare heating is controversial. The various explanations that have been postulated include the following: proton beams that heat the chromosphere without producing a direct HXR signature (Simnett & Haines 1990); anomalous conductive heating by thermal electrons (Takakura 1992); and sudden pinch-heating at the loop top (Feldman et al. 1994).

We consider an alternative explanation whereby the preflare soft X-ray heating is produced by Ohmic dissipation in thin current channels (or sheets) that are aligned parallel to the direction of the magnetic field in the E-W loop. These current channels generate an associated DC–electric field that simultaneously accelerates electrons along the magnetic field to produce impulsive hard X-rays. In the following analysis, we will combine the soft and hard X-ray observations of the 1992 September 6 flare to derive how the DC–electric field strength must have varied in order for this explanation to be plausible.

Holman, Kundu, & Kane (1989) give the following formulae for the total Joule heating rate Q and electron acceleration rate $\dot{N}$ in a field-aligned current system with magnetic field strength B G and associated electric field strength E V cm^{-1}

$$Q = 1.11 \times 10^{21} n_s A_{18} B_2 T_7^{1/2} \nu_e (E/E_D) \text{ ergs s}^{-1} , \quad (2a)$$

$$\dot{N} \simeq 2.83 \times 10^{29} n_s A_{18} B_2 T_7^{-1/2} \nu_e (E_D/E)^{11/8} \times \exp\left[-(2E_D/E)^{1/2} - (E_D/4E)\right] e \text{ s}^{-1} , \quad (2b)$$

where $\nu_e = 10 n_9 T_7^{-3/2}$ s^{-1} is the thermal collision frequency, n_s is the number of current channels, A_{18} cm^2 is the area of individual channels, and $E_D = 7 \times 10^{-6} n_9 T_7^{-1}$ V cm^{-1} is the Dreicer electric field. The numerical subscripts denote the order of each parameter (e.g., $T_7 = T_e/10^7$, etc). For $E < E_D$, the only electrons that runaway are those with velocities above a critical threshold velocity $v_c = (E_D/E)^{1/2} v_e$. In particular, for $E/E_D \ll 0.01$, Joule heating will dominate over acceleration since there are few electrons with velocities above this critical threshold. For increasing values of E/E_D, acceleration will dominate as a larger fraction of the electrons enter the runaway regime and produce increasing nonthermal HXR emission. Ultimately, all electrons will runaway when $E = E_D$. This dependence of increasing HXR emission on increasing runaway rate suggests an empirical relationship $F_{HXR} = \alpha \dot{N}$, where F_{HXR} is the intensity of nonthermal HXR emission produced by the runaway electrons and α is a constant of proportionality that is to determined from the observations.

The relative importance of acceleration versus heating can be parameterized by the ratio $\dot{N}/Q$, which has the useful property that it depends only on T_e, n_e, and E. In particular, given the Ca XIX–derived measurements of T_e and n_e, this ratio provides a novel diagnostic for the unknown electric field strength. Accordingly, we can write

$$F_{HXR}/Q_{obs} = \alpha \dot{N}/Q , \quad (3)$$

where the right-hand term is the theoretical ratio from equations (2a) and (2b), and the left-hand term is the ratio of the observed nonthermal HXR emission to the thermal heating rate implied by BCS soft X-ray observations. We assume that α is constant during the flare and set F_{HXR} equal to the total BATSE count rate intensity summed above 50 keV with the preflare background subtracted. (The emission below 50 keV is excluded in order to minimize possible contamination by thermal emission.) For the temporal variation of E, we assume a simple functional form in which E increased during the HXR rise phase and remained constant after the first peak of hard X-rays. Using T_e and n_e from the soft X-ray observations, we solve first for the constant values of E and α after this first peak. We use a two-parameter least-squares fit of equation (3) to F_{HXR} during the impulsive phase of the flare when BATSE showed the strongest burst emission (i.e., from the time of the first HXR peak to 09:06 UT). Having solved for the constant α after the peak, we perform a backward solution of equation (3) to derive the temporal variation in E from preflare to HXR maximum.

Figure 6*a* shows the results of the fitting process. The computed F_{HXR} is superposed on the BATSE intensity above 50 keV. The computed E during the preflare and impulsive phase is shown in Figure 6*b*. We find that the overall evolution of hard X-rays during the impulsive phase is consistent with a DC–electric field strength that increased montonically from a preflare value of $\lesssim 10^{-5}$ V cm^{-1} to a value of $E = (9 \pm 1) \times 10^{-5}$ V cm^{-1} at the time of the first peak of the HXR burst and remained constant thereafter. The evolution of the hard X-ray emission during the impulsive phase is tied strongly to the variation of the ratio $\epsilon = E/E_D$. Figure 6*b* shows that a factor of 5 increase in ϵ from preflare to HXR maximum corresponds to over a factor of 100 increase in HXR emission. This strong sensitivity is largely due to the exponential dependence of the runaway rate on ϵ (cf. eq. [2b]) which stems from the Maxwellian energy distribution function of the thermal electrons.

The assumption of a unity filling factor in the calculation of n_e implies that the loop volume is filled uniformly with soft X-ray emitting plasma that is at the temperature derived from BCS Ca XIX. It is likely that the flare volume is filamented into finer structures with intrinsically different temperatures and densities. Since the full-Sun BCS instrument averages over the entire flaring active region, the Ca XIX–derived values of T_e and n_e provide lower bounds to the actual temperature and density of finer structures within the loop. Given the computed value of E, we can estimate the filamentation of the DC–electric field current system and its relationship to the coronal filling factor. We use the time of the first HXR peak as the reference point of this calculation. Assuming a laminar sheet geometry, the total volume of n_s current channels is given by $V_s = n_s L_s w_s \delta r$, where L_s is the length, w_s is the width, and δr ($\ll w_s$) is the thickness of individual sheets. We derive δr from the constraint that the self-induction magnetic field of individual current channels must be less than the ambient coronal magnetic field strength.

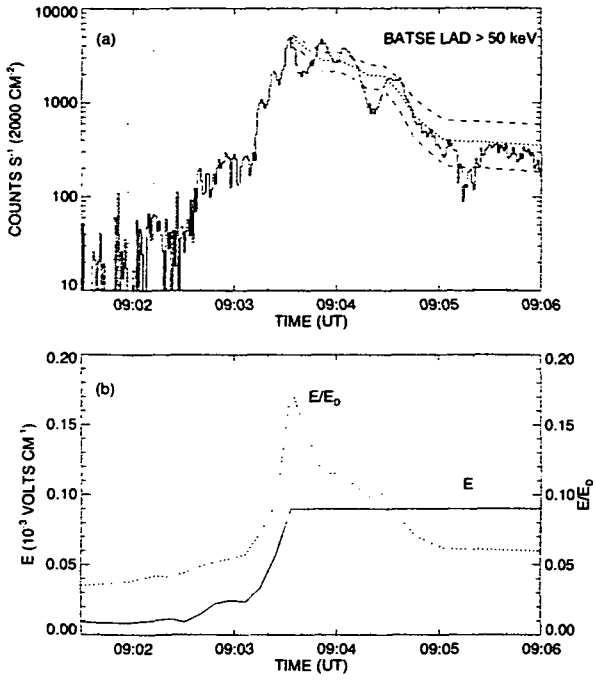

FIG. 6.—(*a*) The total BATSE DISCLA hard X-ray (background-subtracted) count rate about 50 keV. The dotted line shows the least squares best-fit hard X-ray intensity F_{HXR} predicted by the DC-electric field model (eq. [3]) for a constant electric field strength $E = (9 \pm 1) \times 10^{-5}$ V cm^{-1}, where the uncertainty corresponds to ± 1 σ values. The upper and lower dashed lines show the hard X-ray intensity computed for E at the ± 1 σ values. (*b*) The time variation of the best-fit electric field strength E (*solid line*) and the ratio $\epsilon = E/E_D$ (*dotted line*), where E_D is the Dreicer field. Note that E is assumed constant after the first hard X-ray peak. The electric field strength during the hard X-ray rise phase is computed by numerically solving eq. (3) using the constant α derived from the least-squares fit during the impulsive phase after the first HXR peak.

Holman (1985; eq. [8a]) gives

$$\delta r \lesssim 808 B_2 n_9^{-1} T_7^{-1/2} E_D/E \text{ cm} , \quad (4)$$

where B_2 is the coronal magnetic field strength (in 100 G units). Substituting the values of n_8, T_7, and E_D/E at the first HXR peak gives $\delta r \lesssim 30 B_2$ cm and $V_s \lesssim 30 n_s L_s w_s B_2$. The assumption of a unity filling factor implies that the total assembly of sheets uniformly fills the loop volume such that $V_s = V_{obs}$. Adopting a typical coronal field value of 100 G and assuming that the channels extend along the full length of the loop (with w_s and L_s equal to the total loop length $2L_{obs} = 6 \times 10^9$ cm), we derive $n_s \gtrsim 4 \times 10^6$ and $\delta r \lesssim 30$ cm. The observation of HXR emission at opposite footpoints of the coronal loop suggests that a fraction ($\sim 50\%$) of the sheets have field-aligned currents that are directed in opposite directions along the loop.

The ability to observe such thin structures is, of course, beyond the resolution capability of current or proposed instrumentation. However, if we assume that the same number of individual sheets existed before the impulsive phase, then we can estimate the preflare current I_s within each sheet that is required to explain the observed soft X-ray emission by Joule heating. We use the formula $Q_{obs} = JEV_{obs}$, where the right-hand term is the total Joule heating rate and J is the current density. Substituting the values of E and Q_{obs} corresponding to the preflare time 09:01:57 UT, we derive $J = 4.5 \times 10^8$ statamp cm^{-2} or, equivalently, $J = 0.15$ A cm^{-2}. Hence, the current in a single sheet with cross-sectional area $w_s \delta r$ is given by $I_s = J w_s \delta r \simeq 2.7 \times 10^{10}$ A. Invoking a smaller filling factor (< 1) would imply a larger density for the soft X-ray plasma within the sheets and, hence, a greater frictional drag on the thermal electrons. Consequently, stronger electric fields (and, hence, stronger current heating) would be required in order to produce the same nonthermal HXR emission by runaway electrons. An additional consequence of increased density is to elevate the radiative cooling P_{rad}. This enhanced radiative cooling is crucial since it can potentially counterbalance the increased Joule heating by the coronal current, thus restoring the overall heating rate to remain consistent with the observed thermal soft X-ray emission levels.

Finally, we compare our results with those derived by Benka (1991) and Benka & Holman (1992). The latter investigators fit hybrid thermal/nonthermal electron distribution functions to the high-resolution germanium HXR spectra of Lin et al. (1981). Thermal fits to the low-energy component of these spectra indicate "super hot" temperatures of (30–100) $\times 10^6$ K in $\sim 10^4$ current sheets with typical maximum field strengths of 9.9×10^{-6} V cm^{-1}. Such temperatures are considerably hotter than the peak Ca XIX–inferred temperatures ($\sim 20 \times 10^6$ K) used in our analysis. A direct consequence of higher temperatures is that more electrons are available for runaway acceleration and, hence, weaker electric fields and/or fewer current sheets are required to produce the same nonthermal HXR emission.

4. SUMMARY AND CONCLUSIONS

We have explored a new method for analyzing simultaneous soft and hard X-ray observations of solar flares. The method is based on the assumption that the temporal evolution of impulsive hard X-ray emission is related physically to the runaway acceleration rate of electrons in a DC-electric field (Tsuneta 1985; Holman 1985). The ratio of the electron runaway rate to the rate of Joule heating by a field-aligned current is a straightforward function of the temperature, density and electric field strength in the plasma (Holman, Kundu, & Kane 1989). Using Ca XIX soft X-ray spectra to compute the temperature and density, we have solved for the strength and variation of the electric field that is required to simultaneously explain the observed preflare soft X-ray heating and the impulsive phase hard X-ray emission.

We have applied this technique to the flare of 1992 September 6 and developed the following scenario to explain the sequence of hard and soft X-ray observations:

1. Prior to the impulsive phase, the ratio of the DC-electric field to the Dreicer field is sufficiently low that electron runaway acceleration is negligible compared to Joule heating by the coronal currents. Consequently, thermal soft X-ray emission dominates over nonthermal HXR emission. The Joule heating raises the temperature of the loop to produce the enhanced soft X-ray brightening at the loop top and the dominant preflare Ca XIX stationary component. Thermal conduction from the loop top transports energy to the footpoints where it is converted to mass motions, thus, accounting for the preflare soft X-ray Ca XIX blueshifts.

2. During the interval 09:02–09:03 UT, the DC–electric field strength increases. Based on high spatial resolution soft X-ray images, we postulate that this increase is triggered by magnetic reconnection between two intersecting loops. Recent work by Tsuneta (1993) indicates that magnetic reconnection can enhance the field-aligned coronal current and associated

DC-electric field by driving turbulent convective motions in the current sheet that is formed at the reconnection site. We note that the maximum value of $\epsilon = 0.18$ reached during this flare is below the level at which turbulence-induced instabilities (and associated anomalous heating effects) are expected to become pronounced (Tsuenta 1985). The increasing E raises the Joule heating rate, thereby increasing the loop temperature and shifting a greater population of thermal electrons closer to the critical threshold for runaway acceleration. Consequently, an impulsive increase in nonthermal HXR emission is produced as these electrons enter the runaway regime and are accelerated by the enhanced electric field. The bulk of the HXR emission is produced by thick-target interactions as the accelerated electrons propagate along the loop magnetic field from the reconnection site to the chromospheric footpoints. The initial energy deposited by the electrons during the first HXR peak heats the footpoints and fuels additional chromospheric evaporation. This additional evaporation accounts possibly for the secondary peak in the Ca XIX blueshift velocity at 09:03:10 UT (Fig. 4*c*).

3. The density of the loop increases rapidly (Fig. 4*b*) during the impulsive phase as thick-target heating by the runaway electrons and thermal conduction from the Joule-heated loop plasma continue to drive chromospheric evaporation. The increasing density results in a higher value for the Dreicer field. Since E is assumed constant after the first HXR peak, the increase in E_D produces a decrease in ϵ after this peak and a corresponding reduction in the rate of electron runaways. Physically, the effect of increasing n_e is to amplify the frictional drag on thermal electrons thereby inhibiting runaway acceleration (Holman 1985). The net result is a quenching of the nonthermal HXR emission. The consequences of increasing n_e on the HXR behavior were noted by Tsuneta (1985). Applying a DC-electric field model to a flare observed by *Hinotori*, he interpreted the overall evolution of HXR emission as a transition from particle acceleration dominating under low-density conditions early in the impulsive phase to Joule heating dominating in the higher density conditions prevailing later in the flare. He attributed the increase in density to chromospheric evaporation. The present Ca XIX blueshift observations support this scenario.

Our analysis has shown that the relative behaviors of hard and soft X-rays can be understood in terms of simultaneous heating and acceleration in multiple current channels. With several simplifying assumptions, our application of the DC-electric field model has provided a novel diagnostic for measuring the strength and temporal variation of the electric field within these channels, and a method for determining some of the physical parameters of these channels. Crucial questions relating to how such channels are created, whether they are stable, and how the current system is closed in the lower atmosphere are beyond the scope of the present work. Equally important are the issues of the temperature of the plasma within the sheets and the contribution to the overall energy balance due to heating by the runaway electrons themselves. The temperature values inferred from Ca XIX probably underestimate the actual sheet temperature. A more realistic determination can be made in future using BCS observations of Fe XXV–XXVI line transitions. The effect of electron heating can be addressed by relating the electron runaway acceleration rate to the number flux of electrons precipitating into the chromosphere (cf. Lin & Hudson 1976). In particular, spectral fits to high-resolution BATSE spectra can be used to express the observed nonthermal HXR flux in terms of the electron beam parameters, thus, eliminating the proportionality constant α and permitting a more direct solution for the electric field strength (Zarro et al. 1995).

This work was supported by *Compton Gamma-Ray Observatory* Guest Investigator grants NAS5-32064, 32491 and by the Office of Naval Research. We gratefully acknowledge assistance provided by the Compton Science Support Center, and the useful suggestions for improvement made by a referee. We are especially grateful to Gordon Holman and Stephen Benka for stimulating the study described in this paper.

REFERENCES

Antonucci, E., Gabriel, A. H., & Dennis, B. R. 1984, ApJ, 287, 917
Bely-Dubau, F., et al. 1982, MNRAS, 201, 1155
Benka, S. G. 1991, Ph.D. thesis, Univ. of North Carolina, Chapel Hill
Benka, S. G., & Holman, G. D. 1992, ApJ, 400, L79
Canfield, R. C., et al. 1993, ApJ, 411, 362
Culhane, J. L., et al. 1991, Sol. Phys., 136, 89
Doschek, G. A., et al. 1986, in Proc. *SMM* Flare Workshop, Energetic Phenomena on the Sun, ed. M. R. Kundu & B. Woodgate (NASA CP 2439), 4-1
Dreicer, H. 1959, Phys. Rev., 115, 238
Feldman, U., Hiei, E., Phillips, K. J. H., Brown, C. M., & Lang, J. 1994, ApJ, 421, 843
Fishman, G. J., et al. 1989, in Proc. Gamma Ray Observatory Science Workshop, ed. W. N. Johnson (NASA/GSFC), 2-39
Fludra, A., Lemen, J. R., Jakimiec, J., Bentley, R. D., & Sylwester, J. 1989, 344, 991
Heyvaerts, J., Priest, E. R., & Rust, D. M. 1977, ApJ, 216, 123
Holman, G. D. 1985, ApJ, 293, 584
Holman, G. D., Kundu, M., & Kane, S. 1989, ApJ, 345, 1050
Li, P., Emslie, G. A., & Mariska, J. T. 1989, ApJ, 341, 1075
Lin, R. P., et al. 1981, ApJ, 251, L109
Lin, R. P., & Hudson, H. S. 1976, Sol. Phys., 50, 153
Manheimer, W. M., & Klein, H. H. 1975, Phys. Fluids, 18, 1299
Mariska, J. T., Doschek, G. A., & Bentley, R. D. 1993, ApJ, 419, 418
Mariska, J. T., Emslie, A. G., & Li, P. 1989, ApJ, 341, 1067
Mariska, J. T., & Zarro, D. M. 1991, ApJ, 381, 572
McClements, K. G., & Alexander, D. 1989, Sol. Phys., 123, 161
Moghaddam-Taaheri, E., & Goertz, C. K. 1990, ApJ, 352, 361
Roumeliotis, G., Sturrock, P. A., & Antiochos, S. K. 1994, ApJ, 423, 847
Shibata, K., et al. 1993, BAAS, 25, 1187
Simnett, G. M., & Haines, M. G. 1990, Sol. Phys., 130, 253
Spicer, D. S. 1982, Space Science Rev., 31, 351
Takahura, T. 1992, Sol. Phys., 142, 327
Tandberg-Hanseen, E., & Emslie, A. G. 1988, The Physics of Solar Flares (Cambridge: Cambridge Univ. Press)
Tsuneta, S. 1985, ApJ, 290, 353
———. 1993, in Proc. Symp. on New Look at the Sun with Emphasis on Advanced Observations of Coronal Dynamics and Flares, ed. S. Enome & T. Hirayama, Nobeyama, Radio Obs. Rep., No. 360, in press
Yaji, K., et al. 1993, in Proc. Symp. on New Look at the Sun with Emphasis on Advanced Observations of Coronal Dynamics and Flares, ed. S. Enome & T. Hirayama, Nobeyama, Radio Obs. Rep., No. 360, in press
Zarro, D. M., et al. 1995, in prep

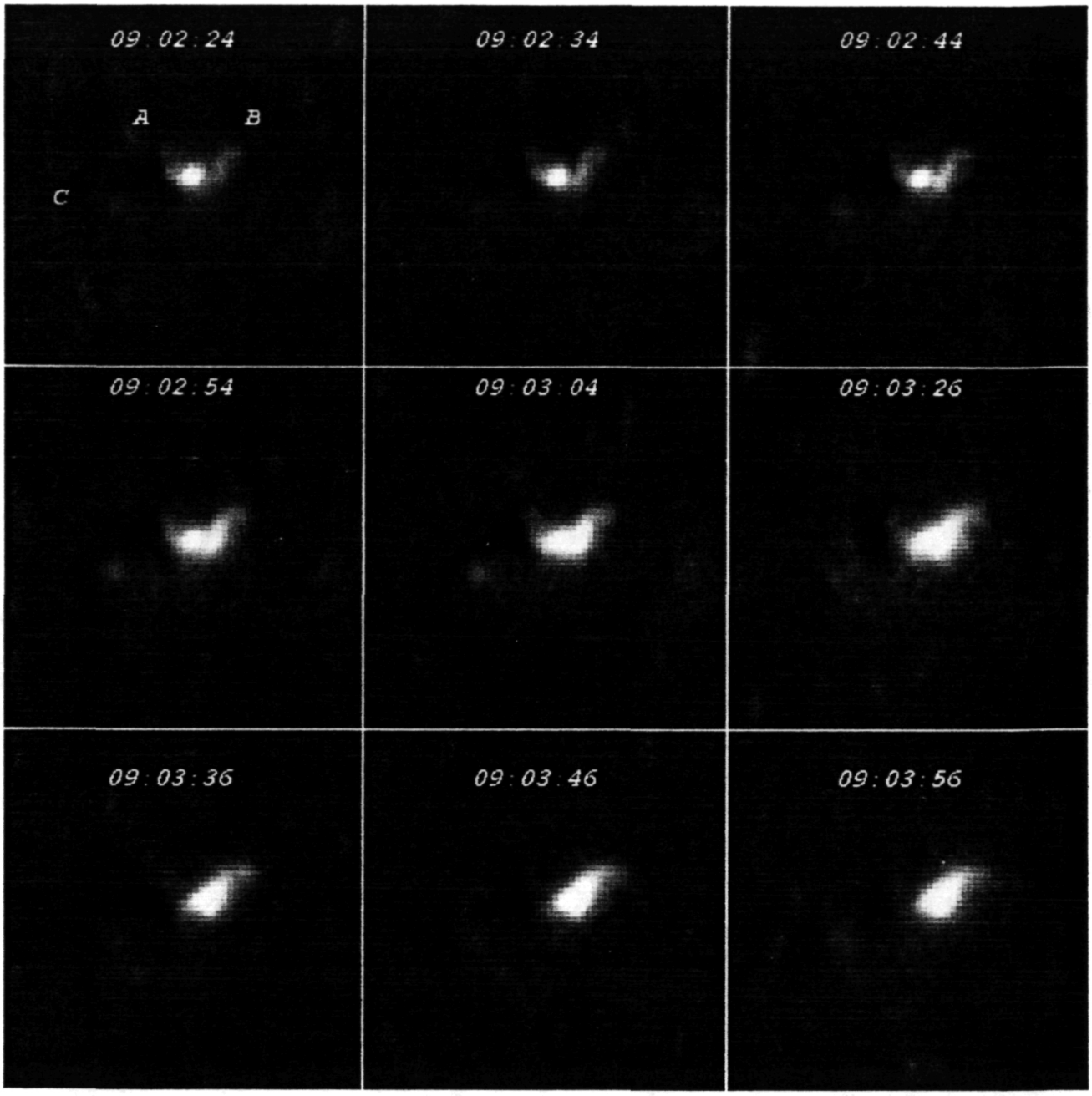

FIG. 3.—A series of *Yohkoh* SXT partial frame Be-filter images at 10 s intervals spanning the initial rise phase of impulsive hard X-rays (09:02:24–09:03:56 UT). *North is up and West is to the right. The images have been normalized to the same exposure times (1 s) and pixel sizes (2.45 arcsec). Each panel consists of* 64 × 64 pixels, corresponding to 157″ × 157″ square. To facilitate relative comparisons, the intensity of each pixel in each image has been renormalized to the intensity of the corresponding pixel in the last image of the sequence at 09:03:56 UT. The sequence of brightenings suggests the interaction of loops: a smaller east-west oriented loop (with footpoints marked A and B) connecting with a larger overlying loop (with footpoints marked C and B). The bright kernel of emission between A and B marks the interaction site. The western legs of the interacting loops show a gradual brightening that commenced at ~09:02:44 UT and increased monotonically during the flare, eventually dominating the total soft X-ray emission from the two loops. This brightening indicates chromospheric evaporation of plasma from the common footpoint B of the two loops.

ZARRO, MARISKA, & DENNIS (see 440, 889)